


# Signatures of wedgelets over Fennoscandia during the St Patrick's Day Storm 2015

Audrey Schillings<sup>1,2,\*</sup> , Laurianne Palin<sup>3</sup>, Gemma E. Bower<sup>2</sup>, Hermann J. Opgenoorth<sup>1,2</sup>, Steve E. Milan<sup>2</sup>, Kirsti Kauristie<sup>4</sup>, Liisa Juusola<sup>4</sup>, Geoff D. Reeves<sup>5</sup>, Mike G. Henderson<sup>5</sup>, Larry J. Paxton<sup>6</sup>, Mark Lester<sup>2</sup>, Maria Hamrin<sup>1</sup>, and Max Van de Kamp<sup>4</sup>

<sup>1</sup> Department of Physics, Umeå University, Linneaus väg, 90187 Umeå, Sweden

<sup>2</sup> School of Physics and Astronomy, University of Leicester, LE1 7RH, United Kingdom

<sup>3</sup> Thales Alenia Space, 26 Av. Jean François Champollion, 31100 Toulouse, France

<sup>4</sup> Finnish Meteorological Institute, Dynamicum Erik Palménin aukio 1, 00560 Helsinki, Finland

<sup>5</sup> Space Science and Applications Group, Los Alamos National Laboratory, Los Alamos, NM 87545, USA

<sup>6</sup> Johns Hopkins University Applied Physics Laboratory, 11100 Johns Hopkins Rd., Laurel, MD 20723, USA

Received 6 October 2022 / Accepted 30 May 2023

**Abstract**—During the long main phase of the St Patrick's Day storm on March 17, 2015, we found three separate enhancements of the westward electrojet. These enhancements are observed in the ionospheric equivalent currents computed using geomagnetic data over Fennoscandia. Using data from the IMAGE magnetometer network, we identified localised field-aligned current (FAC) systems superimposed on the pre-existing ionospheric current system. We suggest that these localised current systems are wedgelets and that they can potentially contribute to a larger-scale structure of a substorm current wedge (SCW). Each wedgelet is associated with a negative  $B_x$  spike. Each spike is recorded at a higher latitude than the former one and all three are very localised over Fennoscandia. The first spike occurred at 17:34 UT and was observed at Lycksele, Rørvik and Nurmijärvi, the second spike was recorded at 17:41 UT and located at Lycksele and Rørvik, whereas the last spike occurred at 17:47 UT and was observed at Kevo and Abisko. Simultaneous optical auroral data and electron injections at the geosynchronous orbit indicate that one or more substorms took place in the polar ionosphere at the time of the wedgelets. This study demonstrates the occurrence of small and short-lived structures such as wedgelets at different locations over a short time scale, 15 min in this case.

**Keywords:** Wedgelets / St Patrick's Day storm / Ionospheric equivalent currents / substorm / westward electrojet

## 1 Introduction

Geomagnetic storms occur mainly due to the interaction of coronal mass ejections (CMEs) from the Sun with the terrestrial magnetosphere, causing strong magnetospheric and ionospheric perturbations. These strong perturbations lead to intense magnetospheric and ionospheric current systems, which provoke strong and fast fluctuations in the geomagnetic field detected on the ground. These magnetic fluctuations in turn create geomagnetically induced currents (GICs) within the ground surface or in any other man-made conducting infrastructures. These induced currents can be responsible for black-outs in power lines, pipelines, railway grids as well as telecommunication systems (Boteler et al., 1998).

During solar cycle 24, one of the biggest storms occurred in March 2015. According to Kataoka et al. (2015) and Guerrero et al. (2017), the strong geoeffectiveness of this storm was due to a combination of a high-speed stream from a coronal hole (CH) and a strong southward magnetic field from a coronal mass ejection (CME). Additionally, right before hitting the Earth, this already combined high-speed stream and CME magnetic field piled up with additional high-density but slow plasma coming from a co-rotating interaction region. This additional structure further enhanced the density and magnetic field of the original solar wind structure. The resulting geomagnetic storm, commonly referred to as “the St Patrick's Day storm”, started on March 17, 2015, at 04:45 UT with a sudden storm commencement (SSC) caused by an increase in the solar wind dynamic pressure and the velocity (Astafyeva et al., 2015; Chemiak et al., 2015), compressing the dayside magnetosphere. Hairston et al. (2016) observed the initial development of the

\*Corresponding author: [audrey.schillings@space.umu.se](mailto:audrey.schillings@space.umu.se)

storm main phase at 06:16 UT when the interplanetary magnetic field (IMF) Bz first turned southward. During about 6 hrs following the onset, the IMF Bz oscillated between  $-20$  and  $20$  nT, before it settled to a more constant negative interval at about 13:00 UT. The main phase of the storm was unexpectedly long,  $\sim 19$  h as reported by many studies, e.g. Hairston et al. (2016), Carter et al. (2016), Guerrero et al. (2017), and Tulasi Ram et al. (2019). In terms of magnetic indices, SYM-H reached a minimum of  $-233$  nT at 22:45 UT and Kp a maximum value of 7+ at 18–21 UT both on March 17 (Astafyeva et al., 2015; Cherniak et al., 2015). Several disturbances in the ionosphere were observed such as thermospheric composition changes in both hemispheres (Astafyeva et al., 2015), phase shifts in the signals of the global navigation spacecraft system (GNSS) due to ionospheric irregularities at mid- and high-latitude (Cherniak et al., 2015; Zakharenkova et al., 2019) and other GNSS disturbances due to an enhanced auroral electrojet (Jacobsen & Andalsvik, 2016). Note that these examples of storm time effects are non-exhaustive and many more detailed consequences of this storm can be found in the literature.

Both in quiet times and during global magnetic storms, short-lived and violent localised magnetic disturbances can occur, which are called substorms (Kamide et al., 1998). One of the main signatures of a substorm is the sudden and localised enhancement of the westward auroral electrojet. Kamide & Kokubun (1996) showed that the auroral electrojet during substorms is composed of two components: 1) a global current system, caused by the two-cell convection pattern, which consists of an eastward auroral electrojet from the evening to pre-midnight magnetic local time (MLT) sector and a westward electrojet from the midnight to morning MLT sector; 2) a localised and intense intensification of the westward electrojet in and around the midnight sector. The global current system is commonly referred to as the DP2 current system. The DP2 current system is also composed of FAC sheets along the auroral oval boundaries, upward (downward) on the poleward edge (Region-1 or R1) and downward (upward) on the equatorward edge (Region-2 or R2) of the evening (morning) sector. The local westward electrojet enhancement around midnight is called the DP1 current system, also related to FACs but localised and upward on the western edge and downward on the eastern edge of the ionospheric current closure. Depending on the MLT sector where the westward electrojet is enhanced, the responsible process of this enhancement can either be the local Hall (and Pedersen) conductivity or the southward electric field component of the global convection electrojet (Ahn et al., 1999). From the pre-midnight to the early morning sector, the Hall conductivity dominates the westward electrojet, whereas, in the late morning, the southward electric field dominates (Kamide & Kokubun, 1996).

The substorm onset, i.e. the initial and localised intensification of the midnight portion of the westward electrojet is often associated with the so-called substorm current wedge (SCW). First introduced by McPherron et al. (1973), the SCW is the initial 3D DP1 current system introduced in the above paragraph. The optical signature of the SCW is a brightening of the auroral emission (Kisabeth & Rostoker, 1973; Kepko et al., 2015), in particular in the vicinity of the upward FAC at its western edge (McPherron et al., 1973). The traditional model of the SCW suggested that the SCW is a large- and wedge-shaped current

system (McPherron et al., 1973; Chu et al., 2014). Following the R1 currents polarity, the SCW associated FAC flows into the ionosphere on the dawnside and in the opposite direction (out of the ionosphere) on the duskside. The FACs are then closed by the westward electrojet enhancement (McPherron et al., 1973). After the substorm onset, the (localised) current wedge expands poleward, eastward and westward, forming the westward travelling surge (WTS) under the upward FAC regions (Oppeanoorth et al., 1980, 1983).

In the last decade, the original SCW model has been revisited and several studies suggested the SCW possibly be composed of several small-scale SCWs called wedgelets (Liu et al., 2018; Nishimura et al., 2020; Ohtani & Gjerloev, 2020). As pointed out by Ohtani & Gjerloev (2020), the original small-scale wedge current system was already introduced by Kisabeth & Rostoker (1974) to describe the discrete expansion of the SCW towards the west in contrast to its more continuous expansion. The expanded FACs associated with an SCW signature are commonly associated with the bursty bulk flow (BBF) (Angelopoulos et al., 1992), whereas, nowadays, the wedgelet model is employed as the ionospheric signature of small-scale magnetotail flux tubes known as dipolarizing flux bundles (DFBs). These localised magnetotail structures are important in the transport of magnetic and energetic flux as well as particle acceleration (Liu et al., 2014, 2016). While energetic transport and particle precipitation are also substorm-related processes, DFBs are mainly observed during the substorm expansion phase. The front of a DFB has a dipolarisation front, where inside of the front, a duskward current and an ion gradient pressure (in some cases an electron gradient pressure has been observed) can be found. Inside the DFB, the geomagnetic Bz component is enhanced in comparison to the ambient plasma from the magnetotail/plasma sheet. A FAC system is associated with DFBs, which in turn is observed in the polar ionosphere. While the SCW is the footprint of a disruption of the cross-tail current (R1) and ring current (R2), the wedgelet is the footprint of an additional small-scale current system associated with a DFB. Multiple earthward DFBs are usually found inside a BBF and are mainly responsible for BBF's magnetic flux transport (Liu et al., 2014). For further details on DFBs, we invite the reader to consult (Liu et al., 2018). Several studies suggested wedgelets observations using spacecraft data (Grocott et al., 2004; Liu et al., 2013; Palin et al., 2015, 2016).

Nishimura et al. (2020) and Ohtani & Gjerloev (2020) investigated whether the SCW could be understood as an ensemble of wedgelets or not. Ohtani & Gjerloev (2020) used the SML index, an equivalent of the AL index but from the SuperMAG database, as a representation of single wedgelets to test the SCW concept. The authors concluded that wedgelets probably contribute to the formation of the SCW although they may not be the primary contribution. Also, Palin et al. (2016) and Nishimura et al. (2020) suggested that substorms do not have one type of SCW system, but rather a composite current system between the traditional large-scale SCW and small-scale and localised wedgelets. Nishimura et al. (2020) concluded that this composite system is probably the most common one and therefore suggested that SCW is not exclusively an ensemble of wedgelets.

In this study, we investigate three particularly sharp and localised variations in the geomagnetic field observed with

ground magnetometers that led to three separate enhancements of the westward electrojets over Fennoscandia. We suggest that these three enhanced westward electrojets are signatures of very short-lived and intense wedgelets. These wedgelets may cause an overall enhancement during the main phase of the St Patrick's Day storm on March 17, 2015. Thanks to the location of Fennoscandia at the time of the storm, we were able to investigate in detail the properties and evolution of the westward electrojet with a variety of instrumentation. The following sections first describe our method and the data used, then we present our observations of the three wedgelets and we conclude with a discussion about the possible contribution of the wedgelets to the main SCW observed by the Defence Meteorological Satellite Program (DMSP) satellite. The last section summarises our findings.

## 2 Data set and method

For this case study, we used several data sets provided by ground-based instruments – magnetometers and All-Sky Cameras (ASC) – and satellites, which are described in the following sections. We studied a specific time interval during the St Patrick's Day storm, March 17 2015 between 17:25 UT and 18:00 UT. That interval is in the middle of the main phase of the geomagnetic storm and the magnetic local time over Fennoscandia was between 19 MLT and 21 MLT. We focused our analysis on this interval because we found three separate enhancements of the westward electrojet. Note that we also looked at the solar wind data from the OMNIWeb database, however, the final calibration does not provide data for the entire storm period (data not shown here). The period of interest is mostly during a data gap. We, therefore, refer the reader to [Cherniak et al. \(2015\)](#), [Astafyeva et al. \(2015\)](#) and [Kamide & Kusano \(2015\)](#) and others reference therein, who employed preliminary calibrated solar wind data only available until the end of 2015.

### 2.1 IMAGE magnetometer network

The IMAGE network is a magnetometer network currently operating 41 stations across Fennoscandia, see [Table 1](#) and [Figure 1](#) ([Tanskanen, 2009](#)). The latitudinal coverage is from 51° N to 79° N, while the network is extended from 4° to 35° in longitude (geographical). The time resolution of the data we employed is 10 s and the coordinate system is defined as *X* toward North, *Y* toward East and *Z* completes the orthogonal system of reference, i.e. positive downwards.

### 2.2 Ionospheric equivalent currents

Using a particular software, developed through the EU-funded ECLAT project, the FMI website also provides the so-called ionospheric equivalent currents calculated from the geomagnetic data recorded by IMAGE magnetometers. The concept of equivalent currents is a model representing the ionospheric currents at a typical altitude of 100 km within a conductive ionospheric E-layer. These 2D virtual ionospheric currents serve as a proxy for the real 3D ionospheric/magnetospheric current system and therefore cause similar perturbations in the terrestrial magnetic field on the ground.

**Table 1.** IMAGE magnetometer stations represented in [Figure 2](#).

Station	IAGA code	GLat	GLong	CGM Lat	CGM Long
Kevo	KEV	69.76	27.01	66.32	109.24
Abisko	ABK	68.35	18.22	65.3	101.75
Rørvik	RVK	64.94	10.98	62.23	93.31
Lycksele	LYC	64.61	18.75	61.44	99.29
Nurmijärvi	NUR	60.5	24.65	56.89	102.18
Uppsala	UPS	59.9	17.35	56.51	95.84
Karmøy	KAR	59.21	5.24	56.43	85.67

*Note.* Glat = geographic latitude, Glong = geographic longitude, CGM = Corrected GeoMagnetic coordinates (model of 2001), <https://space.fmi.fi/image/>.

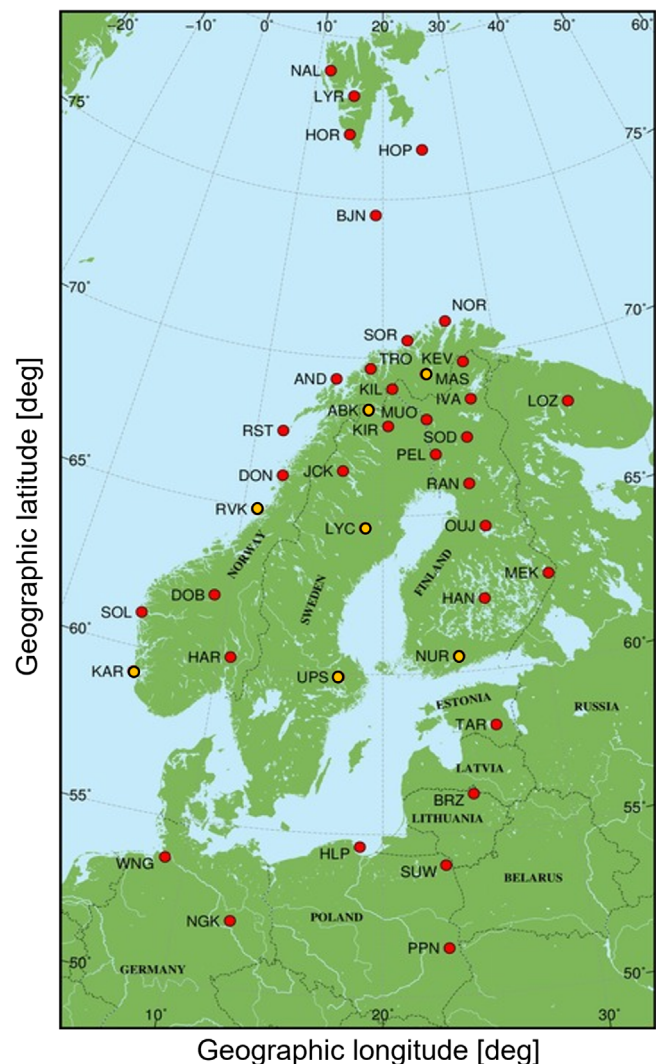


**Fig. 1.** Map of IMAGE network in Fennoscandia including 41 stations at the time of the study. The yellow dots correspond to the stations in [Table 1](#) and [Figure 2](#), whereas the red dots represent the entire network used to determine the equivalent currents in [Figure 3](#) and differential equivalent currents in [Figure 4](#).

The equivalent currents are calculated with the spherical elementary current systems (SECS) method developed by [Amm and Viljanen \(1999\)](#) and [Pulkkinen et al. \(2003\)](#).



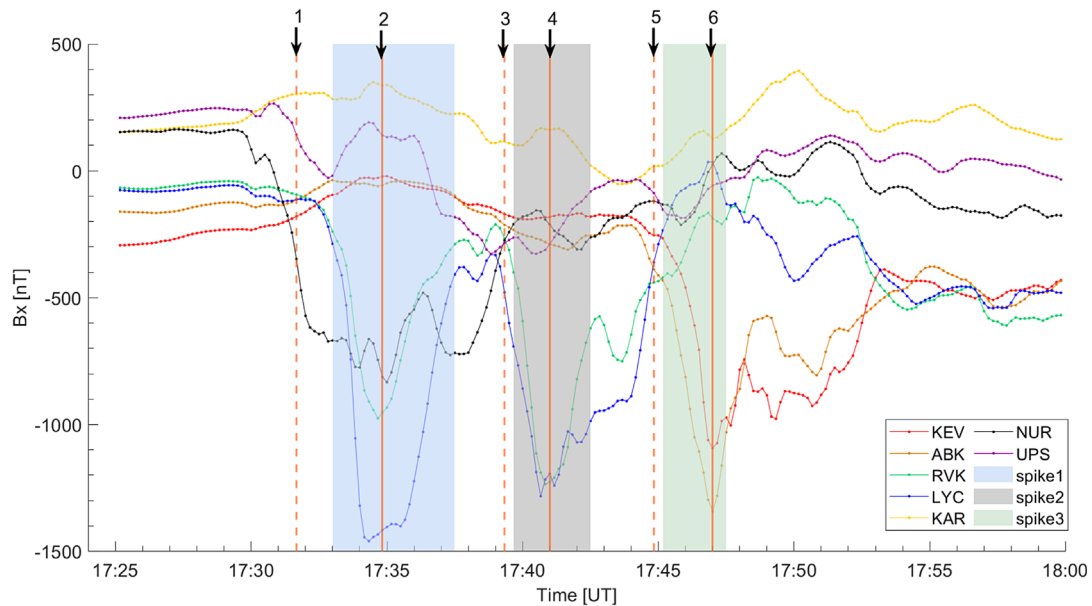


**Fig. 2.** Magnetograms from selected stations of the IMAGE magnetometer network. Each coloured curve represents one station, with KEV being the northernmost station and KAR being the southernmost. The shaded areas refer to the three observed spikes over Fennoscandia. The vertical dashed and solid orange numbered lines mark the times before and at the maximum of the electrojet enhancement respectively. They also refer to the total equivalent currents shown in the six right panels in Figure 3.

During storms and substorms, localised FACs associated with DFBs/BBFs in the magnetotail are superimposed on the existing global system of ionospheric currents and the connected R1 and R2 FACs. As localised FACs can be small in comparison to the pre-existing storm time current systems, the magnetic effects of wedgelets are often hidden under the pre-existing large-scale magnetic perturbations resulting from the global electrojet/FAC system. Subsequently, these localised currents are not easily identified in the equivalent currents during disturbed storms and substorms making the interpretation of the combined magnetic disturbances vectors difficult. In order to extract the spatial and temporal characteristics of these wedgelets from the total equivalent currents, we determined the differential equivalent current vectors (Untiedt et al., 1978; Opgenoorth et al., 1980, 1983b).

The differential equivalent current vectors define the difference in the equivalent currents between the start and the end of a chosen interval. The interval is defined by the sharp onset of growth or decline of a new magnetic disturbance in the 2D ground magnetometer data. Following the reasoning of Untiedt et al. (1978) and Opgenoorth et al. (1980, 1983b), we then inspected 10-second data maps of the magnetic variations over the IMAGE network, showing the differential vectors for each 10-second interval, i.e. the direction and strength of the magnetic changes between two maps (so-called differential vectors). In that data set, we determined when a new current pattern started to develop (first 10-second interval), for how long similar patterns were added, and also when exactly the coherent addition of vectors to the new pattern stopped. We then calculated the complete differential equivalent current vectors for the entire newly appearing (and then disappearing) current systems by defining the end and stop times of the growing and decaying differences in the magnetic disturbances, using the individual

10-second differential maps. From Fukushima's theorem (Fukushima, 1971), the remaining detectable differential magnetic disturbance caused by the wedgelet itself is then mostly due to circular Hall current vortices around the location of the appearing FAC footprints and an additional enhancement of the entire westward electrojet between the up- and downward FAC. Consequently, the localised current systems are typically identified by clockwise (anticlockwise) Hall-current loops corresponding to the footprint of downward (upward) small-scale FACs. See Section 3 for further details about Figures 3 and 4.

### 2.3 All-Sky-Camera

The All-Sky Camera (ASC) images we employed are taken from the MIRACLE network located in Fennoscandia and in Svalbard (<https://space.fmi.fi/MIRACLE/ASC/>). The ASC stations are equipped with electron multiplication CCD (emCCD) cameras that have a field of view of 180 and a green, blue and red filter. The exposure time used in this study is 150 ms for the Kevo and Nyrölä stations in Finland at 69.76 N, 27.01 E and 62.34 N, 25.51 E respectively. Note that the Nyrölä station operated for a test campaign during the storm. We plotted the ASC images in combination with the images from Special Sensor Ultraviolet Spectrographic Imager (SSUSI) on board DMSP (see below).

### 2.4 Satellites

Combined with ASC images, we also looked at the auroral observations taken by the SSUSI on board the DMSP F18 spacecraft (Paxton et al., 2017). On a Sun-synchronous orbit at an altitude of about 830 km, the spacecraft has a period of about



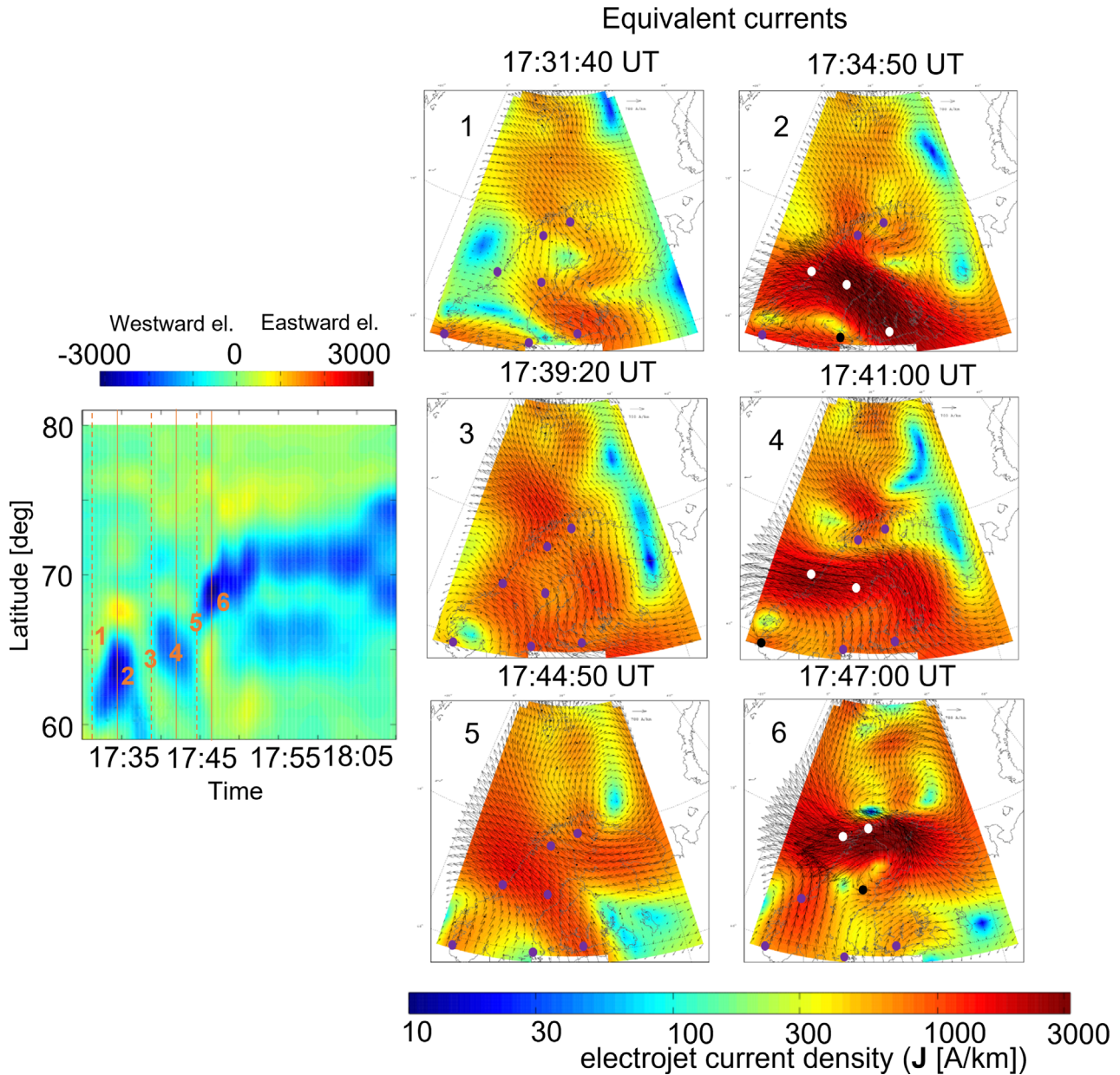


**Fig. 3.** Ionospheric equivalent currents during the main phase of the St Patrick's Day storm, 17 March 2015, from 17:28 UT until 18:10 UT. The left panel shows the evolution of the eastward (red) and westward electrojets (blue) as a function of latitude. The vertical dashed and solid orange lines give the times outside and inside the westward electrojet respectively. The six panels on the right display the total equivalent currents at the time before (panels 1, 3, 5) each of the three electrojet enhancements and at its maximum development (panels 2, 4, 6). The white dots highlight the magnetometer stations that record the  $B_x$  spikes in contrast to the close by stations that did not record any strong perturbations (black dots). On each of the six panels, the purple dots show the remaining stations for comparison.

102 min. The antisunward scans from the SSUSI instrument provide roughly dusk-dawn strips of the polar regions every 20 min. While SSUSI runs on five wavelengths simultaneously, we use the Oxygen line at 130.4 nm (Paxton et al., 1992).

To study the nightside energetic electron flux injections into the geosynchronous orbit, we used the Los Alamos National Laboratories (LANL) 1991-08, 1994-084, 01A, 02A, 04A, 97A satellites. Orbiting on a geosynchronous orbit, the LANL satellites were designed to study energetic particle injections,

which are indicators of substorm activity (Reeves et al., 1996). One of the instruments on board, the Synchronous Orbit Particle Analyser (SOPA), consists of three detector telescopes placed with 30, 90 and 120 angles to the Earth-directed satellite spin axis. The SOPA instrument measures 50 keV–50 MeV protons in 12 energy channels and electrons through 10 energy channels going from 50 keV to approximately 1.5 MeV (Belian et al., 1992). We investigated the 10 electron energy channels with a 1-spin average or about 10-second resolution.

## Differential Equivalent currents

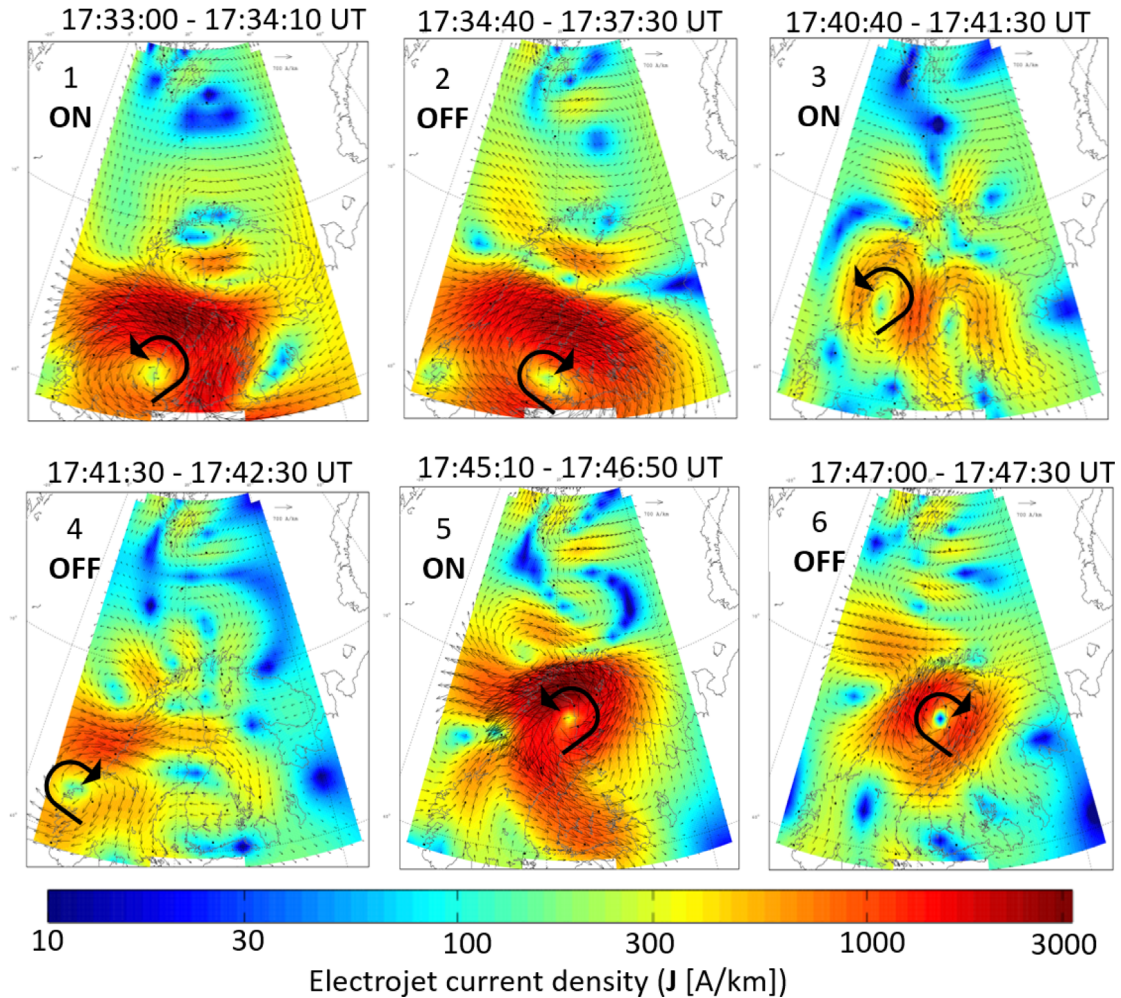


**Fig. 4.** The 6 panels display the differential equivalent currents determined from inspection of individual 10-second data with the FMI IMAGE website. The colour scale gives the intensity of the electrojet current density and the arrows its direction. Panels 1, 3 and 5 show the appearance (ON) of a localised FAC system in contrast to panels 2, 4 and 6 where it vanishes (OFF). The indicated times refer to the interval chosen for the subtraction of the initial and final total equivalent currents to obtain the differential equivalent currents.

### 3 Observations and results

Our results are divided into three subsections. In the [Section 3.1](#), we present the equivalent currents for some Fennoscandian magnetometer stations. In [Section 3.2](#), we focus on the auroral activity before, during and after the electrojet wedgetlets and finally in [Section 3.3](#), we investigate the correlation between the wedgetlet signatures and the geosynchronous satellite data at geostationary orbit, magnetically mapping to sub-auroral latitudes.

#### 3.1 Strong local geomagnetic variations over Fennoscandia

During the main phase of the St Patrick's Day storm, we investigated the magnetograms and corresponding equivalent currents from the IMAGE network over Fennoscandia.

We found several rapid decreases in the  $x$  component of the magnetic field (which we called spikes in the following text), however, one particular sequence of three  $B_x$  spikes associated with three separate westward electrojet signatures caught our attention. These spikes were geographically localised and evolved towards the north over time. The spikes and the corresponding enhancements of the westward electrojet were observed from about 17:30 UT during a time interval of approximately 30 min. The corresponding magnetic local time was around 19 MLT and 21 MLT depending on the geographical location of the station. [Figure 2](#) shows some selected IMAGE magnetometer stations where we observed the  $B_x$  spikes in contrast to other stations located only a few hundred kilometres away where no spikes were recorded. Each coloured curve represents one chosen station in the IMAGE network, whereas the numbered dashed and solid orange lines mark the time before and at the maximum of the perturbations. For these selected times (numbered lines in [Fig. 2](#)), we show the corresponding



equivalent currents over the entire IMAGE network in six (numbered) panels in Figure 3. Back in Figure 2, the shaded areas mark the three spikes observed by the different stations (see Table 1 and Fig. 1 yellow dots). The first  $B_x$  spike (shaded blue – 17:35 UT) is seen at Lycksele (LYC) station with a strong magnetic variation, as well as in Rørvik (RVK) and in Nurmijärvi (NUR) with a smaller disturbance than in Lycksele, whereas Uppsala station (UPS) close by Nurmijärvi does not see the perturbation at all. The second spike (shaded grey – 17:41 UT) is recorded again by Lycksele and Rørvik stations with a similar perturbation but not in Karmøy (KAR) also a nearby station of Rørvik. Finally, the third spike (shaded green – 17:47 UT) is observed at high latitudes in Kevo (KEV) and Abisko (ABK) but not recorded by any of the other stations.

By looking at the latitudes only, we observed the first spike (shaded blue) to occur in south Fennoscandia, the second one (shaded grey) in the middle of Fennoscandia and finally the third one (shaded green) in the north. Further analysis (see below) shows that the three spikes correspond mostly to wedge-like signatures observed in the ionospheric current system.

The overview of the ionospheric system during March 17, 2015, between 17:28 and 18:10 UT is represented in Figure 3 through the total equivalent currents calculated on the FMI website. The left panel (Fig. 3) displays the keogram of the 1D total equivalent currents between 17:28 and 18:10 UT as a function of latitude (58 N–80 N). The colour scale gives the intensity of the electrojet current density  $J$  and the primary direction (blue = westward, red = eastward). We observe three separate and localised enhancements of the westward electrojet (blue patches) before the establishment of a double westward electrojet (starting at 18:05 UT and between 68 and 75 latitude), which is commonly observed during the main phase of a substorm or during the intensification of the current systems in storm times (Gjerloev et al., 2008). The vertical dashed orange lines numbered 1, 3, and 5 mark the times before the sudden appearance of the newly enhanced electrojets and the vertical solid orange lines numbered 2, 4, and 6 mark the times of the maximum development of the new localised current systems in the westward electrojet. The six panels on the right (Fig. 3) display the 2D total equivalent currents over Fennoscandia. The corresponding colour scale gives the strength of the electrojet current density  $J$  (blue = weak, red = strong), whereas the arrows define the direction of the electrojet. The number of each (right) panel refers to the numbered vertical orange lines on the left panel (1D total equivalent currents, Fig. 3) as well as in Figure 2. In Figure 3, the corresponding timings to the vertical orange lines are provided on the top of each (right) panel. On the right panels numbered 2, 4, and 6, the maximum development of each of the new enhancements in the pre-existing westward electrojets occurred at 17:34:50 UT, 17:41:00 UT and 17:47:00 UT. The location where the  $B_x$  spikes were recorded is shown in white dots, whereas black dots show the location where no, or only very small magnetic perturbations were recorded by stations nearby. On each panel, the purple dots show the other stations for comparison. As an example, in panel 2 (Fig. 3) Lycksele, Rørvik and Nurmijärvi (white dots) see an enhancement in the westward electrojet (dark red on the colour scale) while Uppsala (black dot) is in a “hole” (yellow on the colour scale). All other stations are in purple dots. The enhancement of the electrojet is also shown through the first  $B_x$  spike or shaded blue area in Figure 2.

Using the same data as used to produce the total equivalent currents shown in Figure 3, we determined the differential equivalent currents in Figure 4 through the ECLAT software package provided on the FMI website. The colour scale gives the intensity of the electrojet current density  $J$  and the arrows its direction. As the data indicates, three separate magnetic events appeared and disappeared within less than 30 minutes. These events or spikes were most probably caused by very localised transient current structures superimposed on the overall dominating pre-existing and probably slowly enhancing westward electrojet. The 6 panels show the differential equivalent currents vectors for the selected intervals. These intervals represent the successions of appearance (ON) and disappearance (OFF) of the additional localised FAC system hidden in the total equivalent currents. For example, panel 1 gives the Hall current loop corresponding to the footprint of the upward localised FAC (Fukushima, 1971) in the interval 17:33:00 UT to 17:34:10 UT over Lycksele, Rørvik and Nurmijärvi stations, while Uppsala station is at the centre of the loop. Subsequently, Uppsala did not record any variations in its magnetogram as shown in Figure 2. About 3 min later (panel 2, Fig. 4 – OFF), the newly formed current system vanished (clockwise loop). The next current system formed around 17:41 UT but had moved westward and northward over Norway and lasted for about 3 min before it vanished as well (panel 4, Fig. 4 – OFF). Finally, the third enhancement of the westward electrojet formed over northern Sweden for about 1 min (see panels 5 and 6, Fig. 4). We only see the Western signatures of an upward field-aligned current in this event. We note that these three signatures of new magnetic disturbances are located at further and further northern latitudes, indicating quite substantial magnetospheric dipolarisation, of the same order as commonly observed during strong substorms, but within only 5 min at a time. In total these three individual intensification of the magnetospheric ionospheric current system appear to have led to a fully developed storm time substorm, and a resulting electrojet bifurcation (see Sect. 4 for more details).

### 3.2 Auroral features

Besides the magnetograms, we also investigated the ASC images from Nyrölä (NYR) and Kevo (KEV) in Finland. The Nyrölä camera is placed close to Nurmijärvi (NUR) magnetometer station. The camera was in a test campaign during the storm, so we can only use a few images. Figure 5 shows the difference between subsequent images within 30 s of the ASC images from Nyrölä between 17:30:30 UT and 17:33 UT, around the same time we observed the first spike (see Fig. 2, top panel). The colour scale represents the brightening of the aurora, red when the auroral emission is getting brighter and blue when it dims in comparison to the previous image. The first panel (17:30–17:30:30 UT) shows a tongue-like auroral brightening coming from the east, which later disappeared when the aurora filled up the sky (red colour) and moved poleward (panels at 17:31 and at 17:32 UT). The auroral brightening may be an optical signature of an enhanced upward FAC, which leads to higher conductivity. The increased conductivity can then enhance the electrojet in the westward direction for our case, as observed in the equivalent currents and differential equivalent currents.

Despite a very cloudy sky, we also observed an auroral brightening in the Kevo (KEV) ASC in the north of



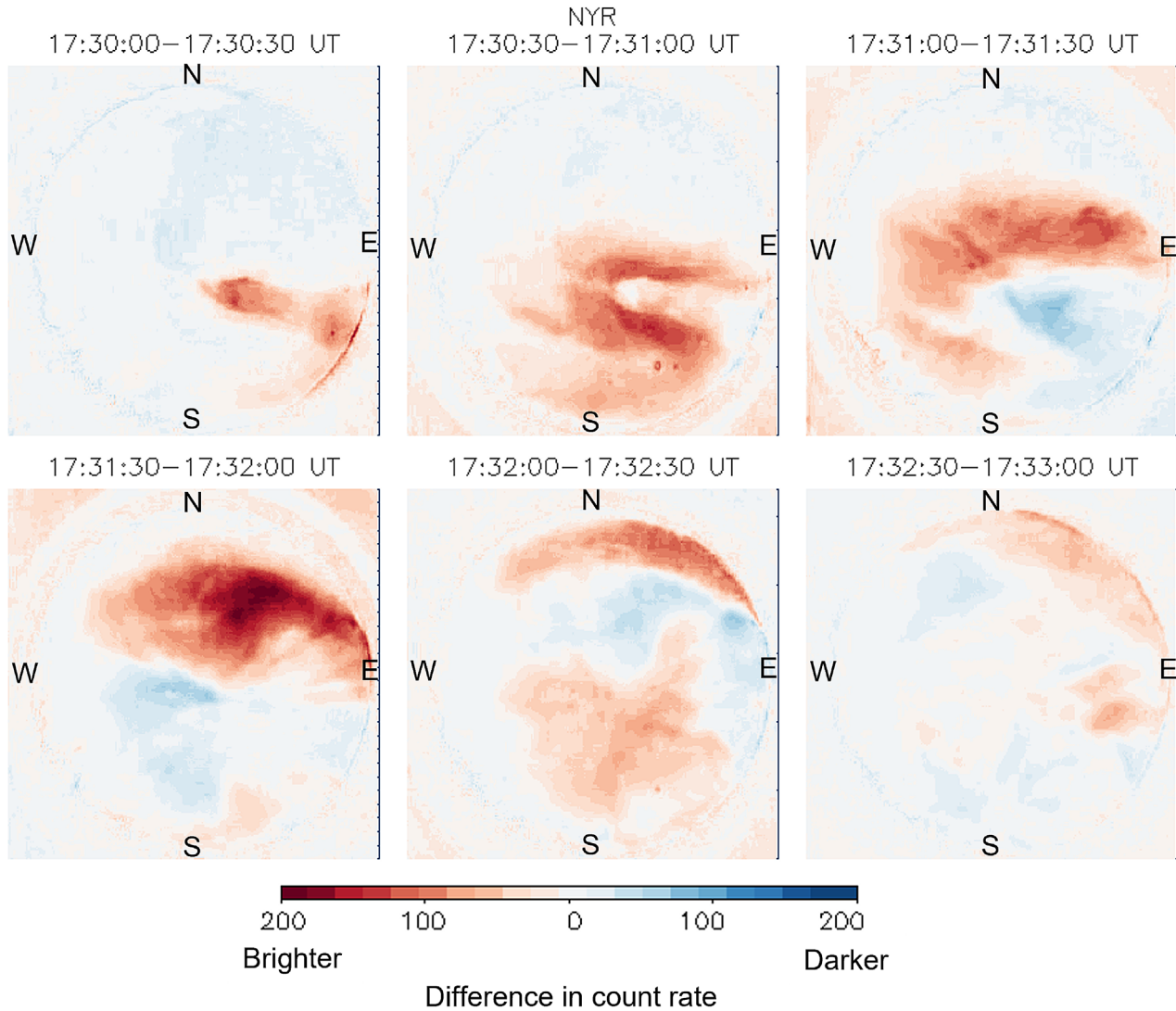


**Fig. 5.** Nyrölä (NYR) All-Sky Camera images on March 17, 2015, between 17:30:30 and 17:33:00 UT (start of the first wedgelet signature in the differential equivalent currents). The colour scale represents the difference in the count rate between two consecutive images within 30 s. Red is showing the brightening of the auroral optical emission.

Fennoscandia during the third enhancement of the westward electrojet (Fig. 4, panel 5). Figure 6 shows the ASC images in Kevo between 17:46:00 UT and 17:47 UT. The colour scale represents the difference in the count rate or the brightening of the auroral emission in 20-second resolution. Red means the emission is getting brighter while blue the emission is weakening, the white or zero counts rate shows the clouds. An auroral brightening is clearly visible (red colour) at 17:46:20 UT. This auroral brightening may be another optical signature for an enhanced upward FAC and therefore the third enhanced westward electrojet.

We also combined the ASC images with the DMSP satellite F18 displayed in Figure 7, March 17, 2015, at 18:00 UT. Figure 7a shows the auroral activity mapped by SSUSI/F18 in the northern hemisphere, we also added Nyrölä station (encircled location). The colour scale represents the radiance intensity on a log scale. The mapping is done using the Altitude Adjustment

Corrected Geomagnetic (AACGM) coordinates and the grid resolution is  $2 \times 2$  latitude. The time in the bottom left of the panel gives the most poleward point of the scan while one scan is completed in approximately 20 min. Figure 7b shows a zoom of the same satellite mapping but with the corresponding ASC Nyrölä image superimposed to the satellite image. Figure 7c displays the ASC Nyrölä image at the same time as SSUSI mapping. We observed an auroral emission in most of the sky, which also corresponds to the double westward electrojet in the equivalent currents (see left panel of Fig. 3) and the main phase of the substorm after the third wedgelet has been observed.

### 3.3 View from the geostationary orbit

The injection of particles at geosynchronous orbit is a known signature of substorms (Mauk & Meng, 1987; Reeves et al., 1996; Liu et al., 2013) even though it is not assumed

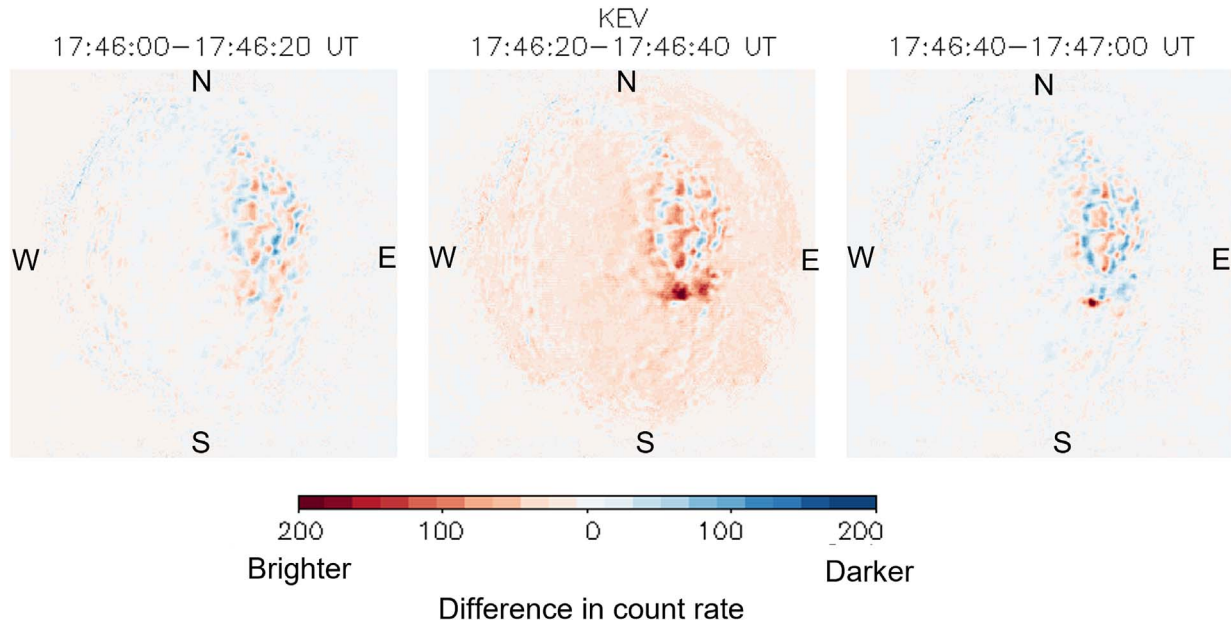


**Fig. 6.** Kevo (KEV) All-Sky Camera images on March 17, 2015, between 17:46:00 and 17:47 UT (third  $B_x$  spike). The colour scale represents the difference in count rate between two consecutive images (20 s). We observe a brightening of the auroral emission (middle panel red colour) during the third enhancement of the westward electrojet in the north of Fennoscandia.

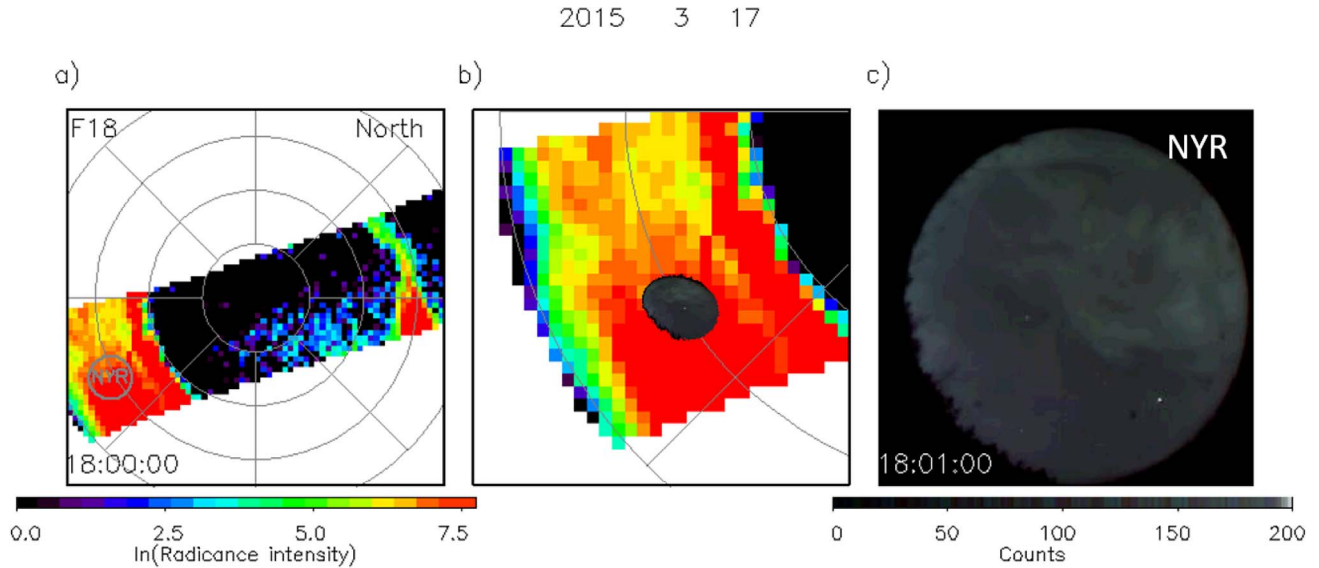


**Fig. 7.** All-Sky camera and DMSP satellite orbits (SSUSI/F18) for March 17, 2015, at 18:00 UT. Panel a) gives the satellite pass mapped by SSUSI on a log scale with a  $2 \times 2^\circ$  latitude and with the encircled locations of the ASC Nyrölä (NYR). Panel b) gives a zoom of the satellite pass with the ASC Images inside the encircled locations superimposed to the satellite images in the northern hemisphere. Panel c) shows the ASC image from Nyrölä.

to be associated with the initiation of a substorm. Figure 8 displays the electron fluxes for six of the LANL satellites. Each coloured line represents one energy channel from approximately 60–280 keV (note that only five energy channels are displayed here for clarity). The left y-axis gives the satellite names, the units are given on the right y-axis. The bottom panel shows the IU and IL index (similar index as AU and AL but using IMAGE stations) during the same period on March 17, 2015,

between 17:00 UT and 18:10 UT. The vertical dashed and solid black lines mark the times before the three enhancements of the westward electrojet and their maximum development respectively, as shown in Figure 3. Additionally, the numbers correspond to the six right panels of the total equivalent currents in Figure 3.

On the top panel in Figure 8, the satellite 01A was in the dawn MLT sector and does not provide complementary

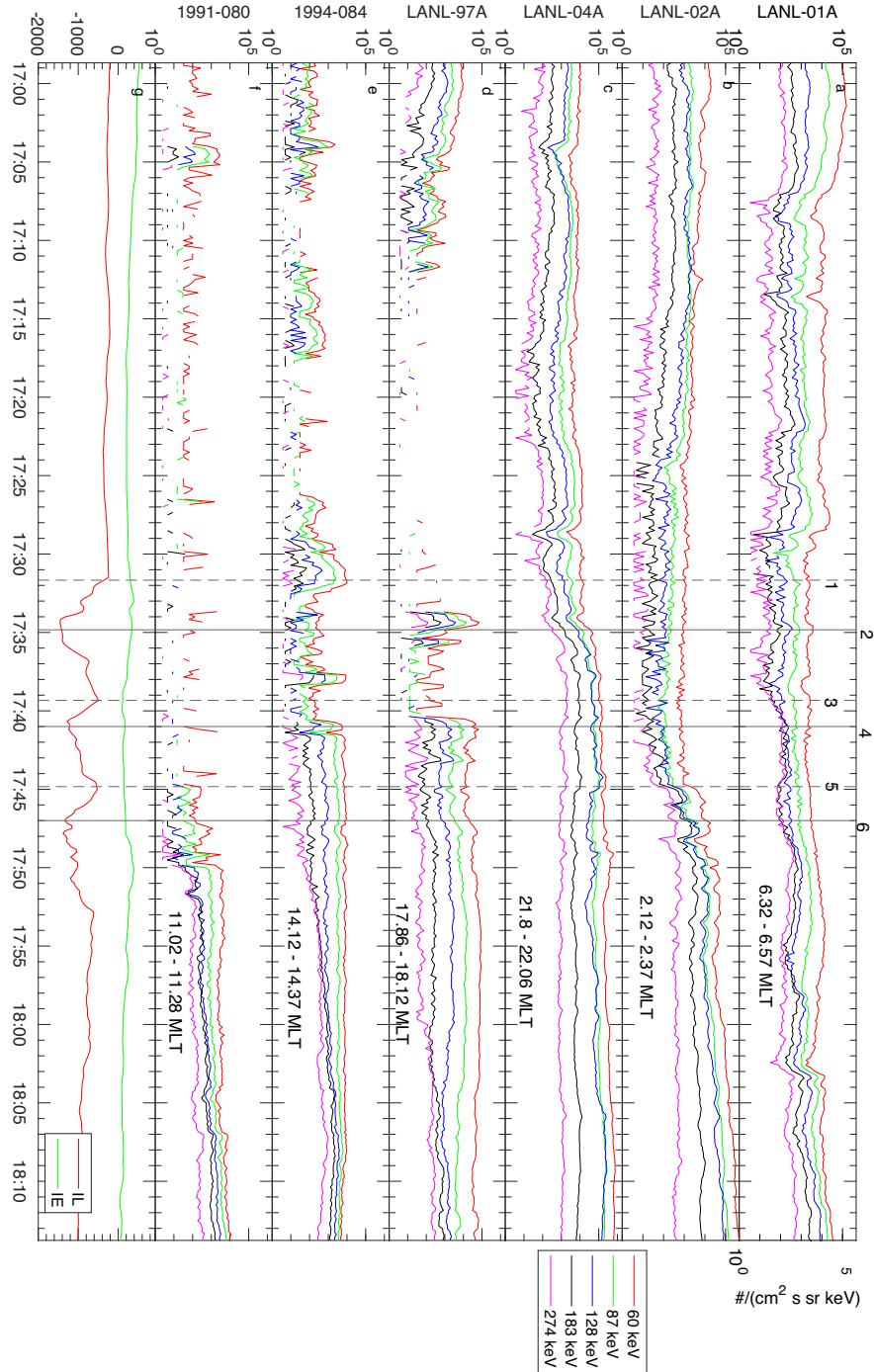


**Fig. 8.** Electron fluxes ( $\sim 60$  to  $\sim 280$  keV) at the geosynchronous orbit by the LANL satellites on March 17, 2015, between 15:00 and 20:00 UT. The six first panels refer each to one satellite (name on the left y-axis) and its measured electron fluxes (each colour is one energy channel). The last panel shows the IU and IL (IMAGE) index for the same period. The vertical dashed and solid black lines correspond to the time before the electrojet enhancement and at their maximum intensity respectively, see also vertical orange lines in Figure 3, left panel (1D equivalent currents) or the numbered right panels.

information for our events. The satellites 02A and 04A (Figs. 8b and 8c) were in the nightside MLT sector  $\sim 02$  MLT and  $\sim 22$  MLT respectively when the electrojet enhancements are observed. The large-scale flux increase suggests one or multiple injections of electrons from the plasma sheet into the inner magnetosphere but the satellites were not well-positioned to directly

observe any dispersionless injections. For the 1st spike at 17:34 UT at LANL 04A, one could interpret an injection and the satellite stays in the dispersion region afterwards. Whereas LANL 02A potentially shows an injection of particles for the 3rd spike (17:47 UT) only. Neither satellites (02A and 04A) show a clear onset of a substorm as we may have expected.



The last three satellites (see panels d, e, and f in Fig. 8) were located in the dusk (97A – ~18 MLT) and dayside (080 – ~11 MLT and 084 – ~14 MLT) MLT sectors respectively. From the discontinuous and very low energy electrons in Figure 8d, 8e and 8d, we see that satellites 97A and 080 are most probably in the magnetosheath region before the first enhancement of the westward electrojet (97A) and until the third enhancement (080). Satellite 084 was oscillating between the two regions (magnetosheath – magnetosphere) but reentered the magnetosphere a few minutes before the first  $B_x$  spike was recorded in Fennoscandia. From the potential magnetosheath crossings by the satellites and their timing difference, we interpret these observations as an external trigger (solar wind driver) such as a relaxation of the magnetosphere coming slightly from the dusk at the corresponding time of the enhanced westward electrojet in the ionosphere.

## 4 Discussion

We observed three separate enhancements of the westward electrojet in the equivalent currents over Fennoscandia (see Fig. 3). These three separate intensification events during the substorm development occurred at 17:34:50 UT, 17:41:00 UT and 17:47:00 UT respectively, or at around 19 MLT and 21 MLT depending on the station geographical location, which is earlier than what we could typically expect for a substorm. Being in the main phase of a geomagnetic storm could explain this early timing. According to Kamide & Kokubun (1996), the westward electrojet can be enhanced either by an increase in the Hall conductivity if located around midnight and early morning sector or by the southward electric field if located in the late morning. Our observations of the electrojet enhancements occurred around 20 MLT and therefore close to the poleward boundary of the Harang discontinuity (Kamide & Kokubun, 1996). Following this reasoning, the Hall conductivity most probably dominates the enhancement of the westward electrojets. This hypothesis is also shared by Guo et al. (2014), who found that conductivity played a significant role in the westward electrojet observed in the pre-midnight MLT sector.

Hidden from the general proxy of the ionospheric current system, localised FAC systems can be observed in the differential equivalent currents. The differential equivalent currents (see Fig. 4) show three appearances and disappearances of localised Hall quasi-loop currents in magnetometer stations over Fennoscandia. These Hall quasi-loop currents correspond to the enhancements of the westward electrojet observed in the general view of the ionospheric current system (equivalent currents, see Fig. 3). We suggest that these signatures in the differential equivalent currents are wedgelets. Wedgelets have previously been observed with *in-situ* data (Grocott et al., 2004; Liu et al., 2013, 2015; Palin et al., 2015, 2016) and several studies tested the hypothesis of the SCW being an association of wedgelets or not (Ohtani & Gjerloev, 2020; Nishimura et al., 2020). It is not entirely understood yet if the wedgelets would then be a fundamental element of the SCW as suggested by Liu et al. (2015) or only partially contributing – as suggested by Nishimura et al. (2020) (see also their Fig. 6 for a schematic). From Figures 7a and 7b, we observed the

passage of a WTS, suggesting a large-scale SCW following Nishimura et al. (2020)'s scenario, just before the observations of the wedgelets in the equivalent currents and differential equivalent currents.

As shown by Fukushima (1971), we observed a series of individual and very localised FAC systems by looking at the differential equivalent currents, which were superimposed on the pre-existing electrojets (see Fig. 4) and compare to Figure 3 – where they are seen as individual westward electrojet enhancements instead of a continuously developing current system that could potentially lead to an SCW (Akasofu et al., 1965). In Figure 3, left panel a continuous westward electrojet only developed after around 17:55 UT. The observation of triple wedgelets makes this event particular because they may occur before the substorm starts or could actually form the stepwise development of the substorm expansion phase (within a storm). This event is particular also because these spikes are very intense, short-lived, and independent from each other. The first wedgelet is very localised in longitude and less in latitude (observed by Lycksele and Nurmijärvi), the second wedgelet is somewhat more extended in longitude than the first one, but similarly narrow in latitude, but at somewhat higher latitude (Rørvik and Lycksele), whereas the last wedgelet is mainly observed by Kevo and Abisko and it is localised both in latitude and longitude. All three wedgelets contain a significant amount of new currents and may be associated with substorm onsets, but far stronger than previously observed in the step-wise onset of individual substorms (Palin et al., 2016). We believe that the magnetospheric processes causing these wedgelets, like e.g. the braking of bursty bulk-flows at the inner earthward edge of the plasma sheet might be much stronger during storm times when that critical location is much closer to Earth. This hypothesis is supported by Angelopoulos et al. (2020), who also found energetic flux increases due to a rapid reconnection event close to the geostationary orbit during a geomagnetic storm in December 2015. The authors observed that these rapid reconnection events led to an energy release of about 36 times stronger than during a regular substorm.

Two other significant substorms occurred during the main phase at around 13:30 UT in the post-midnight MLT sector and at around 23:15 UT in the early morning sector (also observed by Kozyreva et al., 2018), however, none have multiple onsets over Fennoscandia as the potential ~ 17:30 UT substorm does, even though many IMAGE magnetometer stations recorded strong  $B_x$  spikes. According to Kozyreva et al. (2018) data, the substorm over Fennoscandia started at 17:48 UT, which is in accordance with the substorm list created by Newell & Gjerloev (2011) based on the SuperMAG magnetic index (SML). The Newell & Gjerloev (2011) algorithm found a substorm at 17:45 UT over Fennoscandia, whereas Ohtani & Gjerloev (2020), who looked for more localised substorms did not detect any substorms during the period March 17–18, 2015. We believe that this multiple wedgelet observation is associated with the substorm growth or expansion phase, which might have occurred earlier as the IL index dropped from –278.5 nT at 17:20 UT to –1318.5 nT at 17:34 UT. In the substorm list by Newell & Gjerloev (2011), the algorithm detected a substorm onset at 17:20 UT in the morning MLT sector (06 MLT). The IL index indeed indicates a short decrease around 17:20 UT before a significantly bigger decrease around the first wedgelet. This assumption may be supported by three

of the LANL satellite data at the geosynchronous orbit showing some excursion(s) in the magnetosheath before re-entering the magnetosphere successively at the time of the wedgelet observations (see Fig. 8).

Unfortunately the wedgelets occurred too early in the evening MLT sector to have potentially good optical data from the entire MIRACLE ASC network (Fennoscandia). We only have optical data from Nyrölä in the south of Finland that ran for a test campaign and partial data (due to clouds) from Kevo. Figures 5 and 6 show the ASC images from Nyrölä and Kevo respectively. The tongue-like auroral brightening is observed in the Nyrölä images right before the first enhancement of the westward electrojet whereas the sky fills up with aurora during the first wedgelet. Later on Kevo ASC images show a brightening behind the cloud layer during the third wedgelet. We interpreted these auroral emission brightenings as potential optical signatures of enhanced upward FAC and therefore increased conductivity, which then leads to the wedgelets. Figure 7 shows a satellite pass from DMSP satellite F18 in combination with the optical image from Nyrölä in Finland. At 18:00 UT, the DMSP auroral activity does not reveal any particular features, such as auroral streamers or arcs that could be related to the formation of the upward FAC system related to the previous wedgelets. The auroral activity (ASC in Nyrölä and DMSP/SSUSI) mostly suggested that the main phase of the substorm is ongoing.

At the geosynchronous orbit, the LANL satellites located in the dayside MLT sector showed signatures of a possible relaxation of the magnetosphere coming from the dusk side (see Fig. 8d–8f), while the LANL satellites located in the nightside (Fig. 8b–8c) measured injection of electrons in the same time as the enhancement of the westward electrojets were observed. These electron injections could potentially be associated with each of the  $B_x$  spikes, which suggests that intensifications take place in the polar ionosphere.

This example of multiple wedgelets shows that rapid and short-lived variations in the magnetic field outside an expected substorm or storm intensification could lead to harmful damage to power lines or oil pipelines. While we only suggest the impacts on human infrastructures without demonstrating them, Belakhovsky et al. (2019) confirmed the observation of induced GICs in power lines in Karelia and the Kola Peninsula due to what they called impulsive events, events similar to our wedgelets. The authors concluded that in forecasting models to prevent GICs, small scale structures are non-negligible and efforts should be taken to predict GICs more realistically. Following the same reasoning even though not shown here, we would therefore recommend that future models may want to predict energetic BBFs or even more precisely DFBs in the vicinity of the inner edge of the plasma sheet in order to provide warnings of wedgelet signatures and the small FAC systems associated with them.

## 5 Conclusions

During the main phase of the St Patrick's Day storm on March 17, 2015, we found three signatures of wedgelets over Fennoscandia. Using data from the IMAGE magnetometer network, three separate  $B_x$  spikes were recorded over a few magnetometer stations only, whereas other stations did not

observe the spikes at all, as we show in Figure 2. We investigated these signatures further using the equivalent current vectors, which give a proxy for the ionospheric current system. The equivalent currents show three separate enhancements of the westward electrojet within 15 min. Through the differential equivalent current vectors constructed with the ground magnetic field data (see Fig. 4), we observe the switch on (appearance) and switch off (disappearance) of an additional ionospheric current system superimposed to the pre-existing field-aligned current system. This additional and localised current system is detectable through the magnetic field data and due to a quasi-circular Hall current created close to the FAC footprint and an enhancement in the westward electrojet. While the exact nature of the substorm current wedge is not fully understood yet, we suggest that the observed wedgelets are part of a composite current system consisting of a large-scale substorm current wedge as well as wedgelets as suggested by Nishimura et al. (2020). Additionally, we investigated optical data with DMSP/F18 SSUSI instrument and All-Sky camera (ASC). DMSP satellite F18 had one pass in the northern hemisphere right after the signatures of the three wedgelets. The pass shows auroral activity over Fennoscandia but no particular features that could explain the wedgelet signature beforehand. However, from the ASC images at Nyrölä and Kevo, we observed a brightening of the auroral emission during the first and third wedgelets respectively (Figs. 5 and 6). Finally, we investigated the electron injections at geosynchronous orbit, which occurred simultaneously with the  $B_x$  spikes and the associated wedgelets. These possible injections from the satellites located on the nightside may indicate the presence of substorm activity in the polar ionosphere, whereas the satellites on the dayside show signatures of a magnetopause crossing.

This study shows that in approximately 15 min, three spikes associated with strong enhancements of the westward electrojet and with potential optical and magnetospheric signatures occurred at three different and localised parts of Fennoscandia. While our wedgelets are similar to Belakhovsky et al.'s (2019) impulsive events, we also conclude (but did not demonstrate) that these very localised structures could lead to significant localised space weather effects, which will not be predictable from the forecasts due to their small and short-lived structure.

**Acknowledgements.** We thank the institutes who maintain the IMAGE Magnetometer Array: Tromsø Geophysical Observatory of UiT The Arctic University of Norway (Norway), Finnish Meteorological Institute (Finland), Institute of Geophysics Polish Academy of Sciences (Poland), GFZ German Research Centre for Geosciences (Germany), Geological Survey of Sweden (Sweden), Swedish Institute of Space Physics (Sweden), Sodankylä Geophysical Observatory of the University of Oulu (Finland), and Polar Geophysical Institute (Russia). The AE data were retrieved from the OMNIWeb page [https://omniweb.gsfc.nasa.gov/form/omni\\_min.html](https://omniweb.gsfc.nasa.gov/form/omni_min.html). We acknowledge the substorm timing list identified by Newell and Gjerloev technique (Newell & Gjerloev, 2011) and by Ohtani and Gjerloev technique (Ohtani & Gjerloev, 2020), the SMU and SML indices (Newell & Gjerloev, 2011); and the SuperMAG collaboration (Gjerloev, 2012). The MIRACLE network is operated as an international collaboration under the leadership of the Finnish Meteorological Institute. INAF-IAPS maintains the ITACA ASC in Ny-Ålesund, and SGO of the University of

Oulu maintains the ASC in Sodankylä. AS acknowledges the Swedish National Research Council under grant 2021-06683 and AS, HO and LP acknowledge the Swedish National Space Agency (SNSA) for its financial support under grant 10077/15. GEB is supported by the Science and Technology Facilities Council (STFC), UK, studentship. SM and ML are supported by STFC grant ST/W00089X/1. The work of LJ and KK in this investigation was supported by the Academy of Finland (decision 339329). MH is supported by the Swedish National Space Agency grant 81/17 and the Swedish Research Council grant 2018-03623. LP was sponsored by DMSP Special Sensor Ultraviolet Spectrographic Imager (SSUSI) program, contract N00024-13-D-6400, AFOSR grant 26-0201-51-62 Next generation advances in ionosphere thermosphere coupling. The authors do not have any conflict of interest. The editor thanks two anonymous reviewers for their assistance in evaluating this paper.

## References

- Ahn B-H, Emery BA, Kroehl H, Kamide Y. 1999. Climatological characteristics of the auroral ionosphere in terms of electric field and ionospheric conductance. *J Geophys Res Space Phys* **104**(A5): 10031–10040. <https://doi.org/10.1029/1999JA900043>.
- Akasofu S-I, Chapman S, Meng C-I. 1965. The polar electrojet. *J Atmos Terr Phys* **27**(11): 1275–1305. [https://doi.org/10.1016/0021-9169\(65\)90087-5](https://doi.org/10.1016/0021-9169(65)90087-5).
- Amm O, Viljanen A. 1999. Ionospheric disturbance magnetic field continuation from the ground to the ionosphere using spherical elementary current systems. *Earth Planets Space* **51**(6): 431–440. <https://doi.org/10.1186/BF03352247>.
- Angelopoulos V, Artemyev A, Phan TD, Miyashita Y. 2020. Near-Earth magnetotail reconnection powers space storms. *Nat Phys* **16**(3): 317–321. <https://doi.org/10.1038/s41567-019-0749-4>.
- Angelopoulos V, Baumjohann W, Kennel CF, Coroniti FV, Kivelson MG, Pellat R, Walker RJ, Lühr H, Paschmann G. 1992. Bursty bulk flows in the inner central plasma sheet. *J Geophys Res Space Phys* **97**(A4): 4027–4039. <https://doi.org/10.1029/91JA02701>.
- Astafyeva E, Zakharenkova I, Förster M. 2015. Ionospheric response to the 2015 St. Patrick's Day storm: A global multi-instrumental overview. *J Geophys Res Space Phys* **120**(10): 9023–9037. <https://doi.org/10.1002/2015JA021629>.
- Belakhovsky V, Pilipenko V, Engebretson M, Sakharov Y, Selivanov V. 2019. Impulsive disturbances of the geomagnetic field as a cause of induced currents of electric power lines. *J Space Weather Space Clim* **9**: A18. <https://doi.org/10.1051/swsc/2019015>.
- Belian RD, Gisler GR, Cayton T, Christensen R. 1992. High-Z energetic particles at geosynchronous orbit during the Great Solar Proton Event Series of October 1989. *J Geophys Res Space Phys* **97**(A11): 16897–16906. <https://doi.org/10.1029/92JA01139>.
- Boteler D, Pirjola R, Nevanlinna H. 1998. The effects of geomagnetic disturbances on electrical systems at the Earth's surface. *Adv Space Res* **22**(1): 17–27. [https://doi.org/10.1016/S0273-1177\(97\)01096-X](https://doi.org/10.1016/S0273-1177(97)01096-X).
- Carter BA, Yizengaw E, Pradipta R, Weygand JM, Piersanti M, Pulkkinen A, Moldwin MB, Norman R, Zhang K. 2016. Geomagnetically induced currents around the world during the 17 March 2015 storm. *J Geophys Res Space Phys* **121**(10): 10496–10507. <https://doi.org/10.1002/2016JA023344>.
- Cherniak I, Zakharenkova I, Redmon RJ. 2015. Dynamics of the high-latitude ionospheric irregularities during the 17 March 2015 St. Patrick's Day storm: Ground-based GPS measurements. *Space Weather* **13**(9): 585–597. <https://doi.org/10.1002/2015SW001237>.
- Chu X, Hsu T-S, McPherron RL, Angelopoulos V, Pu Z, et al. 2014. Development and validation of inversion technique for substorm current wedge using ground magnetic field data. *J Geophys Res Space Phys* **119**(3): 1909–1924. <https://doi.org/10.1002/2013JA019185>.
- Fukushima N. 1971. Electric current systems for polar substorms and their magnetic effect below and above the ionosphere. *Radio Sci* **6**(2): 269–275. <https://doi.org/10.1029/RS006i002p00269>.
- Gjerloev JW. 2012. The SuperMAG data processing technique. *J Geophys Res Space Phys* **117**(A9): A09213. <https://doi.org/10.1029/2012JA017683>.
- Gjerloev JW, Hoffman RA, Sigwarth JB, Frank LA, Baker JBH. 2008. Typical auroral substorm: A bifurcated oval. *J Geophys Res Space Phys* **113**(A3): A03211. <https://doi.org/10.1029/2007JA012431>.
- Grocott A, Yeoman TK, Nakamura R, Cowley SWH, Frey HU, Rème H, Klecker B. 2004. Multi-instrument observations of the ionospheric counterpart of a bursty bulk flow in the near-Earth plasma sheet. *Ann Geophys* **22**(4): 1061–1075. <https://doi.org/10.5194/angeo-22-1061-2004>.
- Guerrero A, Palacios J, Rodríguez-Bouza M, Rodríguez-Bilbao I, Aran A, Cid C, Herraiz M, Saiz E, Rodríguez-Caderot G, Cerrato Y. 2017. Storm and substorm causes and effects at midlatitude location for the St. Patrick's 2013 and 2015 events. *J Geophys Res Space Phys* **122**(10): 9994–10,011. <https://doi.org/10.1002/2017JA024224>.
- Guo J, Pulkkinen TI, Tanskanen EI, Feng X, Emery BA, Liu H, Liu C, Zhong D. 2014. Annual variations in westward auroral electrojet and substorm occurrence rate during solar cycle 23. *J Geophys Res Space Phys* **119**(3): 2061–2068. <https://doi.org/10.1002/2013JA019742>.
- Hairston M, Coley WR, Stoneback R. 2016. Responses in the polar and equatorial ionosphere to the March 2015 St. Patrick Day storm. *J Geophys Res Space Phys* **121**(11): 11213–11234. <https://doi.org/10.1002/2016JA023165>.
- Jacobsen KS, Andalsvik YL. 2016. Overview of the 2015 St. Patrick's day storm and its consequences for RTK and PPP positioning in Norway. *J Space Weather Space Clim* **6**: A9. <https://doi.org/10.1051/swsc/2016004>.
- Kamide Y, Baumjohann W, Daglis IA, Gonzalez WD, Grande M, et al. 1998. Current understanding of magnetic storms: Storm-substorm relationships. *J Geophys Res Space Phys* **103**(A8): 17705–17728. <https://doi.org/10.1029/98JA01426>.
- Kamide Y, Kokubun S. 1996. Two-component auroral electrojet: Importance for substorm studies. *J Geophys Res Space Phys* **101**(A6): 13027–13046. <https://doi.org/10.1029/96JA00142>.
- Kamide Y, Kusano K. 2015. No major solar flares but the largest geomagnetic storm in the present solar cycle. *Space Weather* **13**(6): 365–367. <https://doi.org/10.1002/2015SW001213>.
- Kataoka R, Shiota D, Kilpua E, Keika K. 2015. Pileup accident hypothesis of magnetic storm on 17 March 2015. *Geophys Res Lett* **42**(13): 5155–5161. <https://doi.org/10.1002/2015GL064816>.
- Kepko L, McPherron RL, Amm O, Apatenkov W, Baumjohann S, Birn J, Lester M, Nakamura R, Pulkkinen TI, Sergeev V. 2015. Substorm current wedge revisited. *Space Sci Rev* **190**(1): 1–46. <https://doi.org/10.1007/s11214-014-0124-9>.
- Kisabeth JL, Rostoker G. 1973. Current flow in auroral loops and surges inferred from ground-based magnetic observations. *J Geophys Res* (1896-1977) **78**(25): 5573–5584. <https://doi.org/10.1029/JA078i025p05573>.



- Kisabeth JL, Rostoker G. 1974. The expansive phase of magnetospheric substorms: 1. Development of the auroral electrojets and auroral arc configuration during a substorm. *J Geophys Res* **79**(7): 972–984. <https://doi.org/10.1029/JA079i007p00972>.
- Kozyreva OV, Pilipenko VA, Belakhovsky VB, Sakharov YA. 2018. Ground geomagnetic field and GIC response to March 17, 2015, storm. *Earth Planets Space* **70**(1): 2061–2068. <https://doi.org/10.1186/s40623-018-0933-2>.
- Liu J, Angelopoulos V, Chu X, Zhou X-Z, Yue C. 2015. Substorm current wedge composition by wedgelets. *Geophys Res Lett* **42**(6): 1669–1676. <https://doi.org/10.1002/2015GL063289>.
- Liu J, Angelopoulos V, Runov A, Zhou X-Z. 2013. On the current sheets surrounding dipolarizing flux bundles in the magnetotail: The case for wedgelets. *J Geophys Res Space Phys* **118**(5): 2000–2020. <https://doi.org/10.1002/jgra.50092>.
- Liu J, Angelopoulos V, Yao Z, Chu X, Zhou X-Z, Runov A. 2018. The current system of dipolarizing flux bundles and their role as wedgelets in the substorm current wedge. In: *Electric currents in geospace and beyond*. Keiling A, Marghitu O, Wheatland M, (Eds.), American Geophysical Union (AGU), pp. 323–337. ISBN 9781119324522. <https://doi.org/10.1002/9781119324522.ch19>.
- Liu J, Angelopoulos V, Zhang X-J, Turner DL, Gabrielse C, Runov A, Li J, Funsten HO, Spence HE. 2016. Dipolarizing flux bundles in the cis-geosynchronous magnetosphere: Relationship between electric fields and energetic particle injections. *J Geophys Res Space Phys* **121**(2): 1362–1376. <https://doi.org/10.1002/2015JA021691>.
- Liu J, Angelopoulos V, Zhou X-Z, Runov A. 2014. Magnetic flux transport by dipolarizing flux bundles. *J Geophys Res Space Phys* **119**(2): 909–926. <https://doi.org/10.1002/2013JA019395>.
- Mauk BH, Meng C-I. 1987. Plasma injection during substorms. *Phys Scr* **T18**: 128–139. <https://doi.org/10.1088/0031-8949/1987/t18/014>.
- McPherron RL, Russell CT, Aubry MP. 1973. Satellite studies of magnetospheric substorms on August 15, 1968: 9. Phenomenological model for substorms. *J Geophys Res* (1896-1977) **78**(16): 3131–3149. <https://doi.org/10.1029/JA078i016p03131>.
- Newell PT, Gjerloev JW. 2011. Evaluation of SuperMAG auroral electrojet indices as indicators of substorms and auroral power. *J Geophys Res Space Phys* **116**(A12): A12211. <https://doi.org/10.1029/2011JA016779>.
- Nishimura Y, Lyons LR, Gabrielse C, Weygand JM, Donovan EF, Angelopoulos V. 2020. Relative contributions of large-scale and wedgelet currents in the substorm current wedge. *Earth Planets Space* **72**(1): 106. <https://doi.org/10.1186/s40623-020-01234-x>.
- Ohtani S, Gjerloev JW. 2020. Is the substorm current wedge an ensemble of wedgelets? Revisit to midlatitude positive bays. *J Geophys Res Space Phys* **125**(9): e2020JA027902. <https://doi.org/10.1029/2020JA027902>.
- Opgenoorth HJ, Oksman J, Kaila KU, Nielsen E, Baumjohann W. 1983a. Characteristics of eastward drifting omega bands in the morning sector of the auroral oval. *J Geophys Res Space Phys* **88**(A11): 9171–9185. <https://doi.org/10.1029/JA088iA11p09171>.
- Opgenoorth HJ, Pellinen RJ, Baumjohann W, Nielsen E, Marklund G, Eliasson L. 1983b. Three-dimensional current flow and particle precipitation in a westward travelling surge (observed during the Barium-Geos Rocket Experiment). *J Geophys Res Space Phys* **88**(A4): 3138–3152. <https://doi.org/10.1029/JA088iA04p03138>.
- Opgenoorth HJ, Pellinen RJ, Kaila KU, Maurer H, Kueppers F, Heikkilä WJ, Tanskanen P. 1980. Ground based observations of an onset of localized field-aligned currents during auroral breakup around magnetic midnight. *J Geophys Res* **85**: 101–115.
- Palin L, Jacquey C, Opgenoorth H, Connors M, Sergeev V, et al. 2015. Three-dimensional current systems and ionospheric effects associated with small dipolarization fronts. *J Geophys Res Space Phys* **120**(5): 3739–3757. <https://doi.org/10.1002/2015JA021040>.
- Palin L, Opgenoorth HJ, Ågren K, Zivkovic T, Sergeev VA, et al. 2016. Modulation of the substorm current wedge by bursty bulk flows: 8 September 2002 – Revisited. *J Geophys Res Space Phys* **121**(5): 4466–4482. <https://doi.org/10.1002/2015JA022262>.
- Paxton LJ, Meng C-I, Fountain GH, Ogorzalek BS, Darlington EH, et al. 1992. Special sensor ultraviolet spectrographic imager: an instrument description. In: *Instrumentation for Planetary and Terrestrial Atmospheric Remote Sensing*, vol. 1745, Chakrabarti S, Christensen AB, (Eds.), International Society for Optics and Photonics, SPIE, pp. 2–15. <https://doi.org/10.1117/12.60595>.
- Paxton LJ, Schaefer RK, Zhang Y, Kil H. 2017. Far ultraviolet instrument technology. *J Geophys Res Space Phys* **122**(2): 2706–2733. <https://doi.org/10.1002/2016JA023578>.
- Pulkkinen A, Amm O, Viljanen A. 2003. Ionospheric equivalent current distributions determined with the method of spherical elementary current systems. *J Geophys Res Space Phys* **108**(A2): 1053. <https://doi.org/10.1029/2001JA005085>.
- Reeves GD, Belian RD, Cayton TC, Christensen RA, Henderson MG, McLachlan PS. 1996. Los Alamos space weather data products: On line and on time. In: *International Conference on Substorms, Proceedings of the 3rd International Conference held in Versailles*, 12–17 May 1996. Rolfe EJ, Kaldeich B (Eds.), ESA SP-389, European Space Agency, Paris, p. 689.
- Tanskanen EI. 2009. A comprehensive high-throughput analysis of substorms observed by IMAGE magnetometer network: Years 1993–2003 examined. *J Geophys Res Space Phys* **114**(A5): A05204. <https://doi.org/10.1029/2008JA013682>.
- Tulasi Ram S, Nilam B, Balan N, Zhang Q, Shiokawa K, Chakrabarty D, Xing Z, Venkatesh K, Veenadhari B, Yoshikawa A. 2019. Three different episodes of prompt equatorial electric field perturbations under steady southward IMF Bz during St. Patrick's Day storm. *J Geophys Res Space Phys* **124**(12): 10428–10443. <https://doi.org/10.1029/2019JA027069>.
- Untiedt J, Pellinen R, Kueppers F, Opgenoorth HJ, Pelster WD, Baumjohann W, Ranta H, Kangas J, Czechowsky P, Heikkilä WJ. 1978. Observations of the initial development of an auroral and magnetic substorm at magnetic midnight. *J Geophys Res* **83**: 41–65.
- Zakharenkova I, Cherniak I, Krankowski A. 2019. Features of storm-induced ionospheric irregularities from ground-based and spaceborne GPS observations during the 2015 St. Patrick's Day Storm. *J Geophys Res Space Phys* **124**(12): 10728–10748. <https://doi.org/10.1029/2019JA026782>.